ACS APPLIED MATERIALS & INTERFACES

Research Article

www.acsami.org

Structure of Arginine Overlayers at the Aqueous Gold Interface: Implications for Nanoparticle Assembly

Louise B. Wright,[†] Nicholas A. Merrill,[‡] Marc R. Knecht,[‡] and Tiffany R. Walsh*[,§]

[†]Department of Chemistry and Centre for Scientific Computing, University of Warwick, Gibbett Hill Road, Coventry, CV4 7AL, United Kingdom

[‡]Department of Chemistry, University of Miami, Coral Gables, Florida 33146, United States

[§]Institute for Frontier Materials, Deakin University, Geelong, Victoria 3216, Australia

Supporting Information

ABSTRACT: Adsorption of small biomolecules onto the surface of nanoparticles offers a novel route to generation of nanoparticle assemblies with predictable architectures. Previously, ligand-exchange experiments on citrate-capped gold nanoparticles with the amino acid arginine were reported to support linear nanoparticle assemblies. Here, we use a combination of atomistic modeling with experimental characterization to explore aspects of the assembly hypothesis for these systems. Using molecular simulation, we probe the structural and energetic characteristics of arginine overlayers on the Au(111) surface under aqueous conditions at both low- and high-coverage regimes. In the low-density regime, the arginines lie flat on the surface. At constant composition, these overlayers are found to be lower in energy than the densely packed films, although the latter case appears kinetically stable when arginine is adsorbed via the zwitterion group, exposing the charged guanidinium group to the solvent. Our findings suggest that zwitterion−zwitterion hydrogen bonding at the gold surface and minimization of the electrostatic repulsion between adjacent guanidinium groups play key roles in determining arginine overlayer stability at the aqueous gold interface. Ligand-exchange experiments of citrate-capped gold nanoparticles with arginine derivatives agmatine and *N*-methyl-L-arginine reveal that modification at the guanidinium group significantly diminishes the propensity for linear assembly of the nanoparticles.

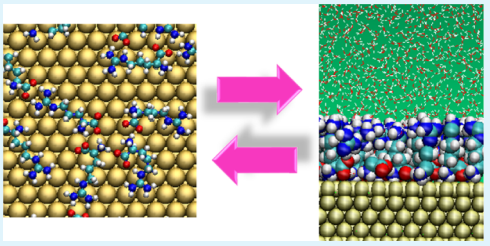

KEYWORDS: *gold, arginine, nanoparticles, simulation, assembly*

INTRODUCTION

Au nanoparticles (AuNPs) possess desirable properties not exhibited by bulk material[1] and hence show promise in a range of possible applications.[2] To prevent agglomeration in solution, AuNPs are typically passivated via adsorption of ligands; this passivation also suggests a means by which the activity of AuNPs could be controlled by surface functionalization.[3] Traditional approaches to passivate AuNPs by thiol-based chemistry have disadvantages including thiol toxicity and nonspecificity (of both material and facet) of binding between the thiol and the metal surface. An alternative approach, via noncovalent displacement of citrate by biomolecules, has become an active area of research, e.g., driving biocombinatorial isolation of gold-binding peptides.[4−7] Thus, new biomolecular passivating ligands that can confer additional functionality are highly sought.[8−10]

It was recently reported that the partial ligand exchange of citrate by the amino acid arginine yielded branched linear chain assemblies of AuNPs.[8,9] To explain this behavior, the authors proposed a hypothesis based on formation of arginine-rich patches on the citrate-passivated surface, with the orientation of arginine within these patches being such that the zwitterion groups of the adsorbates were presented outward. However, the detailed orientation and structural characteristics of amino acid overlayer adsorption at *aqueous* gold interfaces are currently unknown at the atomistic level. This is in contrast to our understanding of the interaction between gold surfaces and molecular adsorbates in vacuo.[11−19]

Molecular simulation has been used previously to study adsorbed overlayers of small molecules onto gold surfaces at the atomistic scale[20−26] with a strong focus on thiol adsorption.[27,28] However, few of these simulation studies have been carried out in the condensed phase; for instance, notably, Cummings and co-workers modeled the adsorption of *liquid* mixtures of tetrahydrofuran and 1,4-benzenedithiolate[20] onto gold. To our knowledge, there have been no reports of atomistic molecular simulations that probe amino acid overlayer formation and structure on gold surfaces under *aqueous* conditions. Modeling and simulation has also been used to investigate segregation and patch formation of coadsorbed molecules on nanoparticles. For example, coarse-grained simulations of the adsorption of surfactants with differing chain lengths or tail groups by Singh et al.[29] reproduced experimentally observed striped microphase

Received: April 7, 2014
Accepted: June 10, 2014
Published: June 10, 2014

separation on the surface of gold and silver nanoparticles and highlighted that segregation was likely to be entropy mediated in that case.[30]

It may be possible that the proposed formation of Arg-rich patches on the surface of the citrate-capped AuNPs could be driven by entropy. In the study of nanoparticle-adsorbed surfactants reported by Singh et al., consideration of enthalpic contributions was neglected. However, neither arginine nor citrate is chemisorbed at the aqueous gold interface, and both are charged, making it likely that enthalpic contributions will compete with these entropic effects in the condensed-phase environment of the overlayer at the aqueous metal interface. Computational evaluation of the entropic contributions to the stability of such overlayers presents an enormous challenge. In a very recent simulation study, Rosa et al.[26] demonstrated that nucleobase overlayers on Au(111) in vacuo were dominated by enthalpic contributions, while adsorption of single nucleobases at the *aqueous* interface was dominated by entropic effects. However, in our study, we seek to investigate the stability of molecular overlayers in the *aqueous environment*; hence, due to the complexity of the system, we confined our simulation study to focus only on the enthalpic contributions. To explore larger system sizes under *aqueous* conditions than would be computationally feasible at the first-principles level, we carried out classical force-field-based molecular dynamics (MD) simulations.

We chose the Au(111) surface as a simple model substrate onto which the adsorption of arginine overlayers could be studied. Although this surface lacks the edges and irregularities present on the surface of an AuNP, it is an appropriate starting point toward building models that are more relevant to experimental conditions, in which nanoparticles of diameter ∼15 nm were used. Thus, the relative length scales of the amino acids and the AuNPs[8,9,31] suggest that AuNP facets can often be acceptably approximated by planar surfaces.[32] A force field for this interfacial system that can reasonably recover biomolecule adsorption on gold is critical to our simulations. Two such families of force fields, CHARMM-METAL and GolP, have recently been developed and used in several studies.[26,33−42] Discussion of the relative merits and limitations of both force fields has been published previously.[26,41−44] Like most atomistic force fields, the dynamic formation and fission of chemical bonds is not within the scope of either force field. Since arginine is not known to chemisorb to gold, we believe an atomistic force-field to be appropriate for the system studied. Thus, here, we used the polarizable GolP force field,[33,34] which was, in part, parametrized and benchmarked against existing in vacuo experimental binding data. At present there is a dearth of definitive, benchmark experimental binding data for small-molecule adsorption at the aqueous Au(111) interface, suitable for evaluating the performance of any biomolecule−gold force field. One such experimental study of the adsorption of phenylalanine at aqueous Au(111) reported a binding free energy,[45] with which previous simulation studies using GolP[35] have shown excellent agreement.

Adsorption of a single arginine molecule at the aqueous Au(111) interface has been investigated previously.[35,36,40] In contrast to these earlier simulation studies,[35,40] here we investigated the effect of more than one amino acid adsorbed at the *aqueous* gold interface. Our specific focus on arginine adsorption is a first step toward exploring the proposed mechanism of arginine-driven AuNP assembly.[8,9] In this previously-proposed hypothesis, it was suggested that arginine-rich surface "patches" formed on the surface of the NPs due to incomplete ligand exchange of the Arg for the adsorbed citrate molecules; it is the atomistic details of arginine within these putative "patches" that we modeled here. The current hypothesis for the linear assembly mechanism of these patchy NPs could be explained either in terms of the dipole alignment or the attraction of the positively and negatively charged patches on the NP surface between adjacent NPs.

Our study focused on the energetics and structural characteristics of arginine overlayers at low- and high-coverage regimes. It is noted that the dynamic deprotonation of an arginine within an interfacial overlayer was not within the scope of the current study, and we assumed 100% protonation of the guanidinium group throughout our simulations. We also considered the relative energetics of both regimes using constant-composition simulations. Our findings suggested a pivotal role regarding exposure of the guanidinium group, which was then further explored via ligand-exchange experiments. The assembly properties and behaviors of citrate-capped AuNPs, displaced with modified analogues of arginine (either agmatine or *N*-methyl-L-arginine), were determined to probe if the linear nanoparticle assembly was altered, either via binding to the gold surface, or through exposure of charged groups to solution.

COMPUTATIONAL METHODS

System Details. Classical MD simulations of arginine overlayers adsorbed onto the Au(111) surface under aqueous conditions were conducted using GROMACS 4.5.4.[46] The GolP force-field[33,34] was used to model a gold slab (29.3 Å × 30.4 Å, thickness of five atomic layers). Since GolP has been parametrized to be compatible with both the bioorganic force-field OPLS/AA[47] and SPC water, these were used to model the arginine and water, respectively.

Two arginine surface coverage regimes, herein referred to as "sparsely packed" (∼1−2 arginines nm^{-2}, 7−14 arginines per simulation cell) and "densely packed" (∼3−4 arginines nm^{-2}, 30−36 arginines per simulation cell), were modeled. For the former (sparsely packed) we considered only one type of arginine−surface orientation in which each arginine lay flat against the surface. In contrast, for high surface coverages, three different types of configurations were considered: one where all molecules were adsorbed to gold via their zwitterion group (labeled "ZI-down"); another with all molecules adsorbed by their guanidinium group (labeled "G-down"); and a third with equal numbers of alternating ZI- and G-down arginines (labeled "alternate" or "A"). For each surface density and arginine−surface orientation, 3 different arginine overlayer configurations were randomly generated; each was subjected to 10.5 ns of annealing prior to production. During this equilibration period, arginine−gold desorption was prevented by restraining the vertical surface−separation distances of the α (CA) and/or guanidinium group (CZ) carbon atoms. Further details of the MD annealing schedule and application of restraints during equilibration are given in the Supporting Information section "Computational Methods and Analysis: Annealing Schedule" and "Determination of CA and CZ Restraining Distances".

For each surface density investigated, the z dimension of the simulation cell was varied such that the water density in the central water layer of the cell (between the gold slab and its periodic image) corresponded to bulk density at 1 bar of pressure. This box dimension (in the range 180.1−184.4 Å) was subsequently used for all simulation cells containing the same total number of arginine molecules. All simulations were conducted in the canonical (NVT) ensemble with three-dimensional periodic boundary conditions. An integration time step of 1 fs was used with coordinates being saved every 1 ps. Post-annealing, simulations were extended by 2 ns with all restraints removed. In all simulations the arginine gold-bound overlayer was solvated by 4625 water molecules at a salt concentration of 0.37 M.

Arginine was modeled as a cation, the protonation state of the amino acid most relevant at pH 7 in solution. The ratio of counterions (Na^+ and Cl^-) was adjusted in each simulation to achieve cell neutrality. Furthermore, steps were taken to ensure that the location of Cl^- ions within the densely packed arginine overlayers did not bias overlayer stability (see Supporting Information section "Computational Methods and Analysis: Cl^- location").

Analysis: Energetics. Energetic analysis was carried out to determine an optimal surface density for arginine in both the sparsely and the densely packed overlayer regimes. At high coverages the energetically most favorable arginine−gold orientation was determined. In order to do this, the average potential energy of the *entire* system (water, gold, and arginines) was obtained from the last 1 ns of each of the three independent simulations at a given arginine surface concentration. The optimal arginine surface density was predicted by calculating the difference in the total potential energy of the entire system between two chemically identical cases containing n arginines: one in which all n arginines were adsorbed onto the gold surface, and the other in which $n - 1$ arginines were adsorbed onto the surface while the n^{th} was free in solution (Figure SI-2, Supporting Information). The free arginine did not interact with the gold or the overlayer. The resulting energy difference is denoted

$$\Delta E_n = E(n_{surf}) - \{E([n-1]_{surf}) + E_{free}\} \quad (1)$$

In an analogous manner, for the densely packed regime only, the difference in the total potential energy of the entire system between ZI-down (E_{ZI}) and either G-down (E_G) or alternate (E_A) overlayers of identical chemical composition was calculated, denoted herein as ΔE_{ZI}.

To compare the relative stability of the dense and sparse packing regimes, a third set of constant-composition simulations was conducted. Each simulation cell contained a total of 33 arginines, with the number of arginines bound to the surface varied from 7 to 14 (adsorbed flat against the surface) and from 30 to 33 (oriented ZI-down). The remaining arginines were placed in solution. Interactions among solution arginines and between solution arginines and the bare gold facet (on the underside of the gold slab) were prevented by fixing one atom in each of the solution arginines in space during equilibration of the system. The vertical surface separation of arginines contained within the overlayer were also restrained, as before, to prevent desorption while annealing. These simulations were then extended with all restraints removed with the average potential energies of the independent triplicate runs determined from the final 1 ns. Further details of the energetic analysis, including estimation of errors, are provided in the Supporting Information section "Analysis: Energetics".

Analysis: Overlayer Properties. For both low- and high-coverage regimes, simulations at the optimal surface density identified by our results (9 and 33 arginines per cell) were extended (bearing in mind the 10.5 ns of equilibration) prior to analysis. In the low-coverage regime, unrestrained simulations were extended by an additional 2 ns to give a total of 4 ns of unrestrained dynamics. However, for the high-coverage regime, where overlayer equilibration is more challenging due to steric limitations, simulations were extended by a further round of annealing (2 ns at 600 K followed by 2 ns at 300 K) followed by an additional 10 ns of unrestrained dynamics. No significant drift in potential energy was observed during the final stages of each simulation (Figure SI-3, Supporting Information). The characteristics of these overlayers with optimal surface density were calculated over the last 2 ns of each simulation. For the densely packed regime only, overlayer characteristics from the last 0.5 ns of the restrained simulations were also calculated to probe possible reasons for the increased stability of one arginine orientation (ZI, G, or A) over the others.

We evaluated the water and Cl^- content in the overlayers, the degree of surface contact in the overlayers and their lateral packing, the average tilt angle of the molecules in the overlayer with respect to the surface normal, and hydrogen bonds between arginines (both zwitterion−zwitterion and zwitterion−guanidinium), including hydrogen-bond time-autocorrelation functions. Full details are given in the Supporting Information section "Computational Methods and Analysis".

EXPERIMENTAL METHODS

Chemicals. Sodium citrate tribasic dihydrate, $HAuCl_4 \cdot 3H_2O$, agmatine sulfate salt, and *N*-methyl-L-arginine acetate salt were purchased from Sigma-Aldrich. All chemicals were used as received. Milli-Q water (18 MΩ·cm, Millipore) was used for all experiments. Molecular structures for arginine, agmatine, and *N*-methyl-L-arginine are shown in Figure SI-4, Supporting Information.

Preparation of Citrate-Capped Au Nanoparticles. The citrate reduction method was used for synthesis of Au nanoparticles.[48] All glassware was washed using aqua regia and Milli-Q water prior to use. A 50.0 mL amount of 1.00 mM $HAuCl_4$ was vigorously stirred until reflux, then 5.00 mL of a 38.8 mM solution of sodium citrate was added. The reaction was refluxed for an additional 15.0 min, where the color changed from clear and colorless to wine red. The reaction was then allowed to cool to room temperature before use.

Au Nanoparticle Assembly. Two arginine analogues, agmatine and *N*-methyl-L-arginine, were used to drive the linear assembly of citrate-capped Au nanoparticles. For each reaction, a varying amount of a 50 mM stock solution of the analogue was added to a 1.00 cm path length quartz cuvette. The concentrations selected represent a 0-, 5000-, 10 000-, 50 000-, and 150 000-fold excess of each analogue in relation to the Au nanoparticles. Samples are referred to as 0K, 5K, 10K, 50K, and 150K, respectively, where K = 1000. Sufficient water was then added to bring the sample volume to 2.40 mL. The nanoparticle assembly was initiated by adding 600 μL of the as-prepared Au nanoparticles to the cuvette, which was then monitored by UV−vis for 2.0 h. The final reaction volume was 3.00 mL with a final Au nanoparticle concentration of 2.0 nM and appropriate secondary ligand concentration.

Characterization. Time-resolved UV−vis spectra were obtained using an Agilent 8453 UV−vis spectrometer employing a 1.00 cm quartz cuvette with a 3.5 mL volume (Starna). All spectra were background subtracted against water, and the cuvettes were cleaned with aqua regia prior to use. Spectra were collected every 20.0 s over a time period of 2.0 h. TEM samples were prepared by adding 5.00 μL of each sample after the 2.0 h reaction time onto 200 mesh Cu grids coated with a thin film of carbon (Ted Pella). TEM samples were then allowed to dry in a desiccator. TEM images were obtained using a JEOL 1400 electron microscope operating at 80 kV.

RESULTS AND DISCUSSION

Sparsely-Packed Arginine Overlayers. *Optimal Arginine Surface Density.* For the range of arginine surface densities investigated in the sparsely packed regime, the differences in the total potential energy of the entire system ΔE_n (eq 1, n = 8−14) were small and comparable in magnitude to their associated errors (Figure 1). In addition, caution must be taken when interpreting the results for $n > 12$ since partial or full arginine desorption events were observed. For example, ΔE_{13} more accurately corresponds to the difference in total potential energy between two systems both consisting of 12 fully adsorbed arginines: one with the 13th molecule still partially bound to the overlayer, and one where this 13th Arg is completely desorbed.

Overall the results from these simulations suggest that within the sparsely packed regime there is little tendency for either arginine adsorption or desorption. Only at n = 9 was there a significant potential energy minimum, and hence, we propose that this is an optimal surface density for a sparsely packed arginine overlayer. All further simulations to characterize the properties of this sparsely packed overlayer (see below), and hence identify the source of its stability, were therefore conducted at this surface density. It is worth noting that for

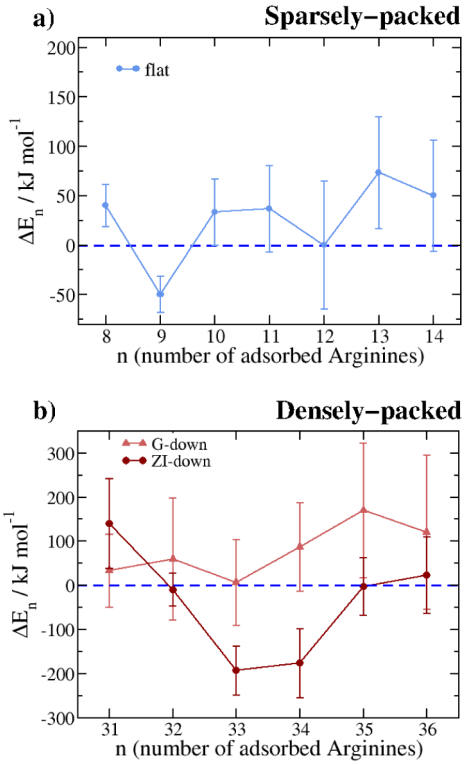

Figure 1. Average difference in total potential energy ΔE_n for arginine overlayers in (a) the sparsely packed regime and (b) the densely packed regime. Negative values indicate it is more favorable to have all n arginines adsorbed than it is for one arginine to be in solution. Note that data for the G-down overlayers were obtained from the final 1 ns of the restrained trajectories; ΔE_n was calculated from the final 1 ns of the simulations after the distance restraints had been lifted in all other cases.

this sparsely packed overlayer not only were each of the arginines adsorbed in a flat configuration similar to that of a single arginine on a bare gold surface,[35,36,40] but also the magnitude of ΔE_n was comparable to the binding energy of a single arginine at the aqueous gold interface (−40 kJ mol^{-1}, see Supporting Information section "Computational Methods and Analysis").

Overlayer Properties. Even after an annealing process amounting to over 15 ns of MD equilibration, significant differences remained in the lateral arrangement of arginines within the three, initially randomly generated, unrestrained overlayers at the optimal surface density of nine arginines per simulation cell (Figure SI-5, Supporting Information). Due to the complexity of this system, it would be computationally prohibitive to identify the definitive global-minimum structure for an aqueous arginine overlayer at this surface density. Hence, to test if a "crystalline-like" arrangement of arginines on the surface was more energetically favorable than these randomly generated ones, we conducted further simulations in which the arginines were initially ordered. Two different ordered overlayer configurations were tested; in both cases the nine arginines were oriented in a head-to-tail manner (see Figure SI-6, Supporting Information). In the "even" configuration, the nine arginines were regularly spaced, while the molecules were clustered closer together in the "close" configuration, leaving a larger proportion of the gold surface exposed. Both of these ordered overlayers were subjected to the same annealing schedule as described earlier, prior to analysis.

Not only were the potential energies of these ordered overlayer systems significantly lower in energy (by more than 100 kJ mol^{-1} (19 mJ m^{-2})) than the randomly generated configurations of the same surface density, but there was also more consistency in other overlayer properties. Since we are interested in characterizing the properties of low-energy overlayer configurations, the results discussed below relate to analysis conducted on these initially ordered configurations. Analogous data for the randomly generated overlayers can be found in the Supporting Information (Figures SI-5 and SI-8, Table SI-1).

Owing to both the small number of different overlayer configurations tested and the limitations of the annealing process, it is entirely possible that even these low-energy configurations are only metastable (Figure SI-9, Supporting Information). However, due to the system complexity we expect that nonideal overlayer configurations may also be kinetically stable under experimental conditions. Taking these caveats into consideration, the average height of both the C_α atoms (denoted CA) and the central carbon atom of the guanidinium group (denoted CZ) above the gold surface during subsequent unrestrained simulations is indicative of how tightly each arginine is adsorbed to the surface (Table 1, Figures SI-7 and SI-8, Supporting Information). In particular, it is noted that the plane of the guanidinium group is parallel to the surface in all cases (Figures SI-5 and SI-9, Supporting Information).

Table 1. Average Properties of Low-Density Arginine Overlayers (surface density 9 arginines per simulation cell)

	"even"	"close"
CA height/Å	4.09 ± 0.70	3.62 ± 0.28
CZ height/Å	3.36 ± 0.20	3.48 ± 0.45
ZI-ZI h-bonds/arginine	0.42 ± 0.05	0.52 ± 0.07
G-ZI h-bonds/arginine	1.16 ± 0.13	1.38 ± 0.08

In addition to the attraction of each arginine within the overlayer for the gold surface itself, we observed hydrogen-bonding interactions between molecules. Both zwitterion−zwitterion and guanidinium−zwitterion hydrogen bonding were optimized within the four-arginine star-like motifs found in our simulations of the initially ordered overlayers (Figure SI-9, Supporting Information). However, even when data from the randomly generated arrays were included in the analysis, the average total number of hydrogen bonds (1.5−2.0 hydrogen bonds per Arg) is significant (Table 1 and SI-1, Supporting Information).

Hence, we propose that at a surface density of nine arginines per cell (∼1 arginine nm^{-2}) arginine−gold and arginine−arginine interactions are optimal; both contribute to overlayer stability. Lower arginine−surface concentrations limit formation of an interfacial hydrogen-bonded network, while repulsion between guanidinium groups on adjacent molecules destabilizes overlayers of surface densities greater than ∼1 arginine nm^{-2}.

Densely-Packed Arginine Overlayers. *Preferred Arginine Orientation.* The average potential energy of overlayers comprising arginines, initially arranged vertically, oriented G-down (Figure 2b), ZI-down (Figure 2c), and alternate (A, consisting of equal numbers of G-down and ZI-down) were obtained from the last 1 ns of the restrained MD simulations. Since the unrestrained overlayers exhibited varying degrees of surface desorption, to provide a fair comparison we conducted

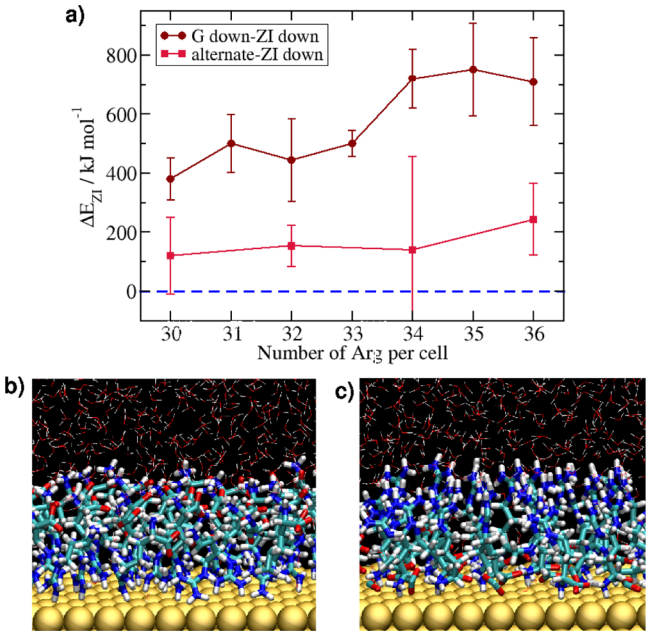

Figure 2. (a) Average differences in the total potential energy, ΔE_{ZI-G} and ΔE_{ZI-A}. In this case all data was obtained from the final 1 ns of the restrained portion of the simulations. (b and c) Simulation snapshots from G-down and ZI-down densely packed overlayers, respectively (34 arginines per simulation cell).

this analysis to probe the orientational preference of arginine on the restrained rather than unrestrained overlayers. In contrast to our arginine surface-density energetic analysis, (Figure 1), the differences between E_{ZI} and E_G were sufficiently large after the annealing process to allow firm conclusions to be drawn.

It is evident from Figure 2a that ZI-down overlayers are energetically favored, by 380 kJ mol^{-1} (71 mJ m^{-2}) or more, compared to the G-down system, over the entire surface density range investigated (~3−4 arginines nm^{-2}). This corroborates evidence from our simulations carried out in the preparatory stage, in which desorption of arginines from G-down overlayers was observed more frequently than from the ZI-down systems. As the surface density is decreased our data suggest a trend for G- and ZI-down overlayers to become energetically comparable. This is expected since at lower surface densities arginine has an increasing tendency to tilt and ultimately lie flat on the surface. To explore whether alternate overlayers would be more energetically stable than either pure G- or ZI-down, randomly generated alternating overlayers were simulated. Our findings show qualitatively that mixed arrays have intermediate stability between G- and ZI-down (Figure 2a).

The average number of hydrogen bonds between adjacent zwitterionic groups was consistently greater for the ZI-down overlayers than for G-down (1.5−2.0 and 1.0−1.5 per Arg, respectively, Figure SI-10a, Supporting Information); we suggest this to be one of the main factors contributing to the prevailing stability of the ZI-down overlayer. From visual inspection, arginines in the ZI-down overlayer were oriented to optimize zwitterionic hydrogen-bond interactions close to the surface, driving a 2D *hcp*-like arrangement of the CA atoms (Figure SI-11, Supporting Information). It is not possible to rule out that defects in this *hcp* array were not solely an artifact of the periodicity of the simulation cell being incommensurate with that of the close-packed lattice. A similar arrangement of ZI groups within G-down overlayers was not observed, possibly as a result of their greater conformational freedom when not bound to the surface. It is noted that even in unrestrained simulations the zwitterion and guanidinium groups of ZI- and G-down overlayers, respectively, exhibited motion restricted roughly to two dimensions due to steric effects and dense packing. Competition for zwitterion−zwitterion hydrogen bonding from liquid water above the overlayer (1.0−2.0 and 0.0−1.0 hydrogen bonds per molecule for G- and ZI-down overlayers, respectively, Figure SI-10b, Supporting Information) and the close approach of positively charged guanidinium groups on adjacent arginine molecules in the G-down overlayers were also thought to have contributed to the destabilization of this orientation relative to ZI-down.

Identification of an Optimal Arginine Surface Density. Although for the densely packed regime the potential energy differences ΔE_n (eq 1, n = 31−36) were greater than that for the sparsely packed regime (Figure 1) again only qualitative conclusions can be drawn due to the large spread in total system potential energies for samples of identical composition and setup. For the G-down overlayers, our energetic analysis evaluated trajectories from restrained runs only due to the tendency for desorption in this case when unrestrained. For the ZI-down overlayers, with their high stability, the data presented was taken from analysis of the unrestrained runs. These calculations agree with the results above, indicating an energetic preference for arginine to adsorb ZI-down in dense overlayers; specifically, there was no statistically significant driving force for arginine adsorption or desorption when adsorbed G-down. For ZI-down, on the other hand, arginine adsorption is energetically favorable within the surface density range 33−34 arginines per cell (~4 arginines nm^{-2}).

Taken together, our results indicate that an optimum densely packed arginine overlayer comprises arginine adsorbed in the ZI-down orientation at a surface density 33 arginines per cell (~4 arginines nm^{-2}). The characteristics of this surface density for the densely packed regime is discussed herein.

Overlayer Properties. In each of the three different randomly generated starting configurations (denoted run 1, run 2, and run 3) of ZI-down overlayers, none of the arginines had fully desorbed after 10 ns of unrestrained dynamics. However, similar to the sparsely packed regime, there were slight differences in the characteristics of each of the three runs.

Each unrestrained MD run was more than 100 kJ mol^{-1} (19 mJ m^{-2}) more stable than its restrained counterpart. Vertical as well as lateral motion of the CA atoms was required for full overlayer relaxation, although the difference between the average CA−surface separation and the restraint distance (4.0 and 3.8 Å, respectively) was minimal. The trends in the total system potential energy for the three runs (run 3 < run 1 < run 2) correlated with observed overlayer stability; run 3 was the most favorable energetically and featured no partial arginine desorption within the time scales probed (Table 2). In terms of structural characterization, analysis of Au−CA (~4 Å) and Au−CZ (~9 Å) distances and tilt (~20°) angles (Figure SI-12a,b, Supporting Information) suggest that all the arginines remained oriented ZI-down and relatively upright within the overlayers.

Due to arginine possessing both charged hydrophilic groups and a hydrophobic alkyl chain, we anticipated that water could play an important role in arginine overlayer stability at the aqueous Au(111) interface. Figure 3a shows that water penetrated all the way through the overlayer, giving rise to a

Table 2. Average Overlayer Properties: Number of Directly, $N(Arg)_{dir}$, and Indirectly Adsorbed, $N(Arg)_{in}$, Arginines and Number of Water Molecules within the Whole Overlayer, $N(w)_{tot}$, and Just Those Associated with Arginine CA Atoms, $N(w)_{CA}$, Calculated over the Last 2 ns of the Unrestrained Trajectories for the Three High-Density ZI-down Arginine Overlayers at Optimal Surface Coverage[a]

	run 1	run 2	run 3
$\langle N(Arg)_{dir} \rangle$	31.95 ± 0.01	32.99 ± <0.01	33.00 ± 0.00
$\langle N(Arg)_{in} \rangle$	1.05 ± 0.01	0.01 ± <0.01	0.00 ± 0.00
$\langle N(w)_{tot} \rangle$	24.87 ± 0.12	31.52 ± 0.40	37.86 ± 0.28
$\langle N(w)_{CA} \rangle$	8.16 ± 0.03	8.93 ± 0.06	11.14 ± 0.07

[a]Errors estimated using block averaging.[51]

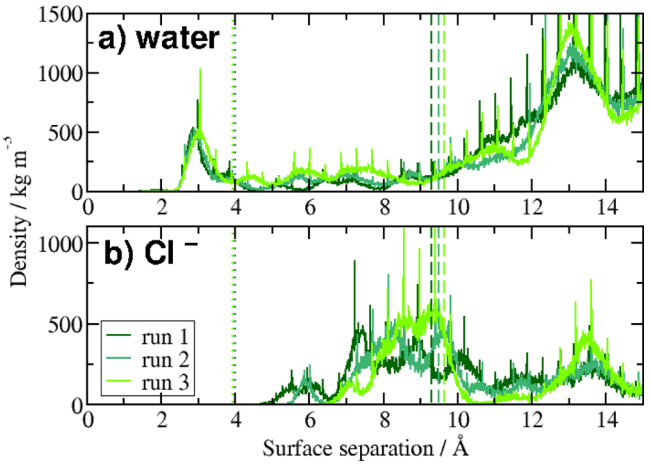

Figure 3. (a) Water and (b) Cl^- vertical density plots as a function of surface separation for molecules within or just above densely packed ZI-down arginine overlayers of surface density 33 arginines per cell. Average CA (dotted line) and CZ (dashed line) distances are included to indicate the relative position of molecules within the overlayers.

local maximum in water density located between the gold surface and the CA atoms (an average of 8−11 water molecules per simulation cell, Table 2). At this surface separation, water could interact with the charged zwitterion groups. As expected, water density is minimal within the middle of the overlayer. However, water does not appear to shield the positively charged guanidinium groups from one another, since water density commensurate with the average CZ atom height is low. This is likely due to the high Cl^- ion density in this region, displacing the water molecules (Figure 3b). We found little evidence of direct Cl^-−Au interaction preventing or disrupting formation of the arginine overlayers, in agreement with the relatively weak adsorption of chloride ions onto gold observed experimentally[49] and predicted from first principles.[25] In the liquid water above the overlayer, there appeared to be at least one structured water layer, most likely due to the positively charged guanidinium groups.

The dense hydrogen-bonded zwitterion−zwitterion network at the surface, found during the restrained portion of the trajectory (Figure SI-11, Supporting Information), was maintained after overlayer equilibration with an average of ∼1.75 hydrogen bonds being formed per arginine (Figure SI-12c, Supporting Information). Although zwitterion−water hydrogen bonding varied more between the three runs, it was consistently less pronounced (∼1 hydrogen bond per arginine, Figure SI-12c, Supporting Information). In general, both types of hydrogen bond, arginine−arginine and arginine−water, had longer persistence times than those found between water molecules (Figure SI-13, Supporting Information) as might be expected due to the charged nature of the zwitterion functional group. Details of further hydrogen-bond analysis are given in Supporting Information section "Densely-Packed Regime−Hydrogen-Bonding Analysis".

Preferred Arginine Overlayer Packing Regime. Our constant-composition simulations of 33 arginines per cell indicated that the sparsely packed overlayer regime was significantly lower in total potential energy (by more than 1000 kJ mol^{-1}, 190 mJ m^{-2}) than the densely packed one (Figure 4). Within error, this analysis also further suggests there

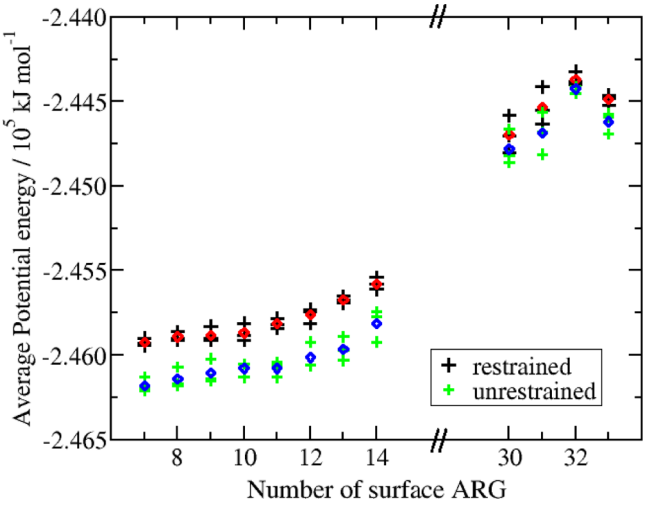

Figure 4. Average total potential energies taken from the last 1 ns of restrained and unrestrained trajectories for systems of identical composition, containing 33 arginines in total, but with varying numbers of arginines adsorbed onto the gold surface. Red and blue diamonds denote the average potential energy of the three independent simulations at each point for restrained and unrestrained overlayers, respectively.

is little driving force for arginine adsorption or desorption within the range of surface densities investigated in the sparsely packed regime (Figure 1a). The structural stability of arginine overlayers in densely-packed regime observed in our simulations, when in a ZI-down configuration, leads us to suggest that overlayers of high surface coverage may yet be metastable, once formed, and hence relevant to experiment.

It should be noted that the results from the restrained simulations provide a better measure of the relative stability and allow like-for-like comparison. For example, at fixed composition with low surface density, there is necessarily a high concentration of arginines in solution. Under these conditions it became challenging to prevent both solution arginine−arginine and arginine−gold interactions (on the underside of the gold slab). Extension of these simulations into lower surface-adsorbed densities was not feasible since our maximum system size could not prevent all of these unwanted interactions.

Although we noted no full arginine adsorption events during our unrestrained constant-composition simulations at low surface densities on the time scales probed, several solution arginines interacted with the overlayer via hydrogen bonding. While direct modeling of the dynamics and mechanism of the overlayer formation process is not computationally feasible,

visual inspection of these simulations suggested insights into the possible formation mechanism. As the surface density increased from the low-density value, it became more likely for the zwitterion group to partially desorb, while the guanidinium remained adsorbed flat. Our results suggest that at intermediate surface densities guanidinium-adsorbed overlayers are more likely until the packing density increases above a threshold such that the guanidinium groups can no longer lie flat at the interface and hence are moving to an upright G-down arrangement. From our energetic analysis, such overlayers would be unfavorable with respect to the ZI-down configuration. Hence, we propose that the substantial overlayer rearrangement, required to transform from a ZI-down densely packed overlayer to G-down (flat) overlayer of intermediate surface coverage, could be the source of the metastability of the former observed here.

Ligand-Exchange Experiments. Since in the high-density packing regime the zwitterion is predicted to be bound to the particle surface, thus exposing the guanidinium group to solution, modification to either region should directly impact the citrate-capped AuNP linear assembly process during exchange with the biomolecule. To this end, we employed both agmatine and *N*-methyl-L-arginine as substitutes for the standard arginine amino acid to observe changes to the assembly process. These molecules have a nearly identical structure as arginine (see Figure SI-4, Supporting Information); however, for agmatine, the alpha-carboxylic acid is removed, while for *N*-methyl-L-arginine, the guanidinium group is methylated. These two species were specifically chosen to determine which component more significantly alters the assembly process: ZI group binding to the AuNP surface (agmatine) or through the solution-exposed cation (*N*-methyl-L-arginine) driving aggregation with negatively charged citrate "patches" on adjacent NP. Similarly, if arginine-rich "patches" of low, rather that high, surface density form on citrate-capped AuNP then it is hypothesized that the change in overall protonation state (from cationic to neutral) of the exchanging ligand, on substitution of arginine for either agmatine or *N*-methyl-L-arginine, could impact on the linear assembly process.

Figure 5 presents the AuNP assembly analysis using agmatine. For this reaction, 2.0 nM citrate-capped AuNPs in water were exposed to selected equivalents of the modified biomolecule. As a control, when no agmatine was mixed with the AuNPs, Figure 5a, no assembly was evident with only randomized orientations of the nanoparticles observed on the TEM grid surface. Furthermore, no change in the optical properties was noted, as anticipated. When agmatine was added to the same system to reach an agmatine:nanoparticle ratio of 5K (5K = 5000), assembly of the materials was evident. As shown in the left panel of Figure 5b, a significant change in the UV−vis absorption properties of the materials was evident. To this end, as the reaction was allowed to proceed, growth of a secondary peak at 665 nm was observed. TEM analysis of these structures after a 2.0 h reaction time demonstrated formation of short linear chains of AuNPs. Consistent with previous studies using arginine, this linear assembly process likely arises from incomplete ligand-exchange processes with the original citrate passivant, resulting in self-segregation of the bound molecules.[9,50] As such, a dipole is imparted across the materials, which drives linear nanoparticle assembly. This is consistent with the UV−vis absorbance that demonstrated formation of two plasmon bands arising from the transverse and linear axes of the assembled materials.

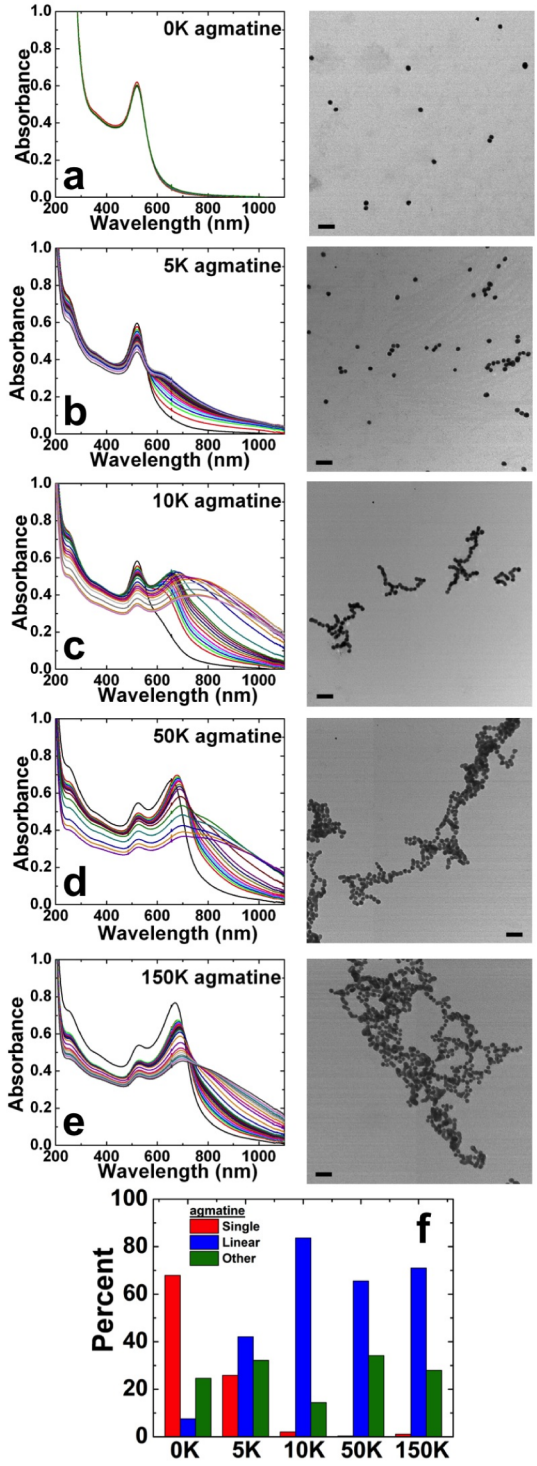

Figure 5. Citrate-capped Au nanoparticle assembly analysis using agmatine at agmatine:Au nanoparticle ratios of (a) 0K, (b) 5K, (c) 10K, (d) 50K, and (e) 150K. UV−vis analysis is shown on the left, while TEM analysis of the assembled materials after 2.0 h is shown on the right (scale bar = 50 nm). (f) Comparison of the assembly state of the materials.

As the agmatine:AuNP ratio was increased, enhanced nanoparticle assembly was observed. For instance, at a ratio of 10K, the UV−vis absorbance of the secondary peak rapidly increases. After 0.5 h, the new peak begins to progressively red shift and broaden. TEM analysis of the materials confirms formation of a more substantial assembly process. This effect

likely arises from an initial dimerization event, which results in the first secondary peak, followed by aggregation of the dimers to form longer chains that drive peak shifting and broadening. This process continues to increase at higher agmatine:nanoparticle ratios; however, at the highest ratio studied, the rate of secondary peak growth and shifting decreases. Under these conditions, more substantial nanoparticle surface coverage occurs using the secondary molecule, thus diminishing the dipole magnitude and the overall assembly process.

When the secondary ligand was switched to *N*-methyl-L-arginine that modified the guanidinium group, a substantial change was observed in the assembly process as shown in Figure 6. Here, no significant linear chain formation was observed until an *N*-methyl-L-arginine:nanoparticle ratio of 50K, which was still quite minimal. At a higher ratio studied, 150K, more substantial assembly was noted; however, it was still lower than the results observed with agmatine above and arginine previously. Note that in the TEM analysis of the 150K *N*-methyl-L-arginine sample a significant degree of particle aggregation was observed. This likely arises from the drying process necessary to prepare the TEM sample. In this situation, the solvent is evaporated, thus greatly increasing the reaction concentration, which has been suggested previously to artificially assist in driving linear assembly.[9] As such, UV–vis analysis is more reflective of the actual reaction under the standard conditions.

Taken together, these two assembly processes indicate that modification at the guanidinium group, as is the case for the *N*-methyl-L-arginine ligand (see Figure SI-4, Supporting Information), significantly hinders nanoparticle linear assembly. This is indicated by a substantial decrease in the rate of particle assembly via the *N*-methyl-L-arginine species as compared to the agmatine sample where the guanidinium group was unchanged but the termini were modified (Figure SI-4, Supporting Information); the results for this latter adsorbate were similar to those found for the parent arginine ligand. This likely arises from changes at the particle surface, in combination with alterations with the distal regions of the ligand interface. In this regard, modification of the guanidinium is anticipated to change the surface charge, thus diminishing the dipole imparted across the particle, leading to slower linear assembly.

These experimental findings indicate the exposure of the guanidinium to be highly influential on the assembly propensity of citrate-capped AuNPs in the presence of arginine. Our simulation data are perhaps best reflective of a scenario relating to formation of an arginine-rich patch, where our simulations have attempted to describe the possible structure inside such a patch. Here, our simulations have not accounted for any possible effects arising from coadsorption of citrate and arginine molecules together. Nor did we consider the driving forces to form such arginine-rich patches on the surface, the size of which (and thus the influence exerted by the boundary effects) could dictate the patch stability, density, and orientation. To make closer connections with these experimental findings, in the future, both the pure citrate overlayer at the aqueous gold interface should be modeled, as should the mixture of the two species coadsorbed. However, to our knowledge, no comprehensive study of the simulated structure of citrate overlayers at the *aqueous* gold interface has been reported to date. Furthermore, overlayers such as these, formed at the aqueous interface, also present challenges for their in situ experimental observation. For example, common techniques such as atomic force microscopy (AFM) are typically applied to

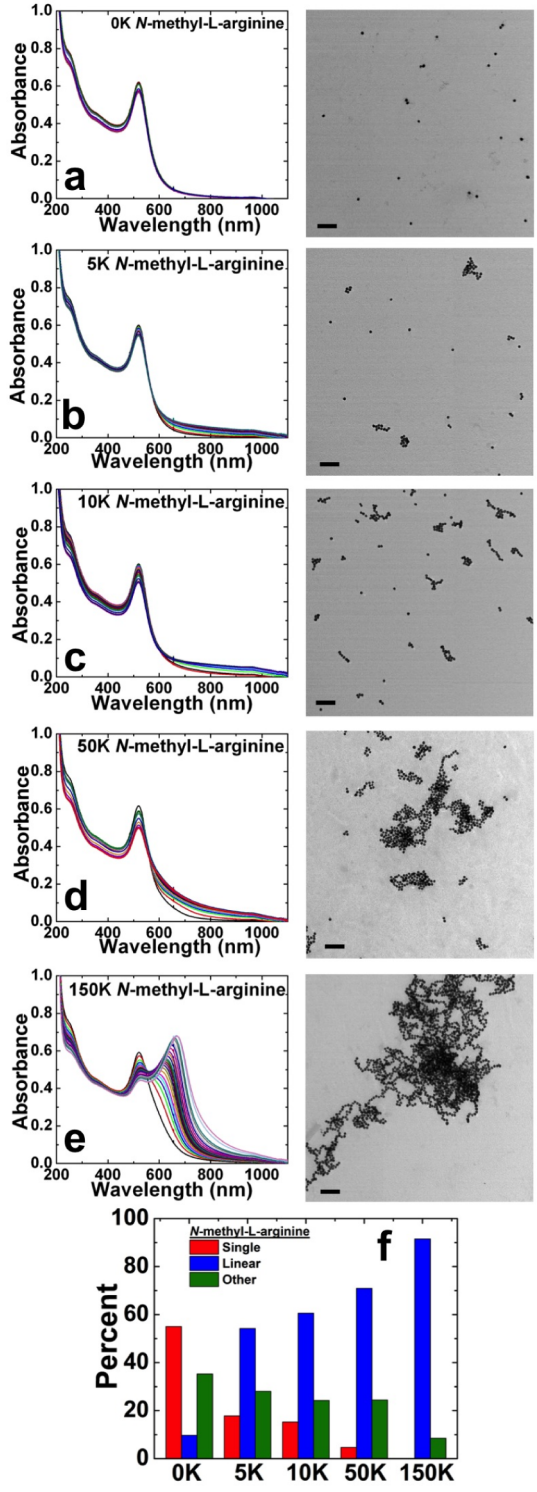

Figure 6. Citrate-capped Au nanoparticle assembly analysis using *N*-methyl-L-arginine at *N*-methyl-L-arginine:Au nanoparticle ratios of (a) 0K, (b) 5K, (c) 10K, (d) 50K, and (e) 150K. UV–vis analysis is shown on the left, while TEM analysis of the assembled materials after 2.0 h is shown on the right (scale bar = 50 nm). (f) Comparison of the assembly state of the materials.

dried samples. Unfortunately, the act of drying the sample may substantially impact the overlayer morphology, not only because of capillary forces present during drying, but also because the interfacial structuring of the liquid water itself may contribute to the overall stability of the overlayer. Therefore,

such AFM images may not be representative of the scenario under aqueous conditions.

In summary, the current hypothesis to explain the linear assembly mechanism of AuNPs observed in experiment[8,9] invokes the idea of partial ligand exchange, resulting in putative formation of Arg-rich and citrate-rich patches on the AuNP surface. Consequently, the assembly mechanism could then be explained either by dipole alignment or by attraction of the positively and negatively charged patches between adjacent AuNPs. According to our simulations, Arg-rich patches on the AuNP surface, in both the sparsely and the densely packed regimes, would present an overall positive charge outward, able to electrostatically interact with a negatively charged citrate-rich patch on an adjacent AuNP. It might be possible that both packing regimes for arginine could be simultaneously present on an Au surface. However, if and how the presence of adsorbed citrate can influence the structure of the arginine overlayer structure remains an open question. Further experimental and computational studies are required to fully elucidate these details.

CONCLUSIONS

From atomistic MD simulations of both sparsely and densely packed arginine overlayers adsorbed at the aqueous Au(111) interface we predict that arginine will preferentially be adsorbed flat with an optimal surface density of approximately ∼1 arginine nm^{-2}. Inter-arginine hydrogen-bonding and guanidinium−surface interactions are likely to be a major source of overlayer stability. Our simulations also suggest a metastable, densely packed arginine overlayer (∼4 arginines nm^{-2}) in which arginine is preferentially adsorbed via its zwitterion group, presenting the positively charged guanidinium group outward into the solvent. The influence of the possible outward presentation of the guanidinium on AuNP linear assembly was further probed by experimental characterization. The ligand-exchange experiments reported here indicated that modification of the guanidinium group led to a diminished propensity for the nanoparticles to form linear assemblies, suggesting a key role of the guanidinium group in the overlayer structure. Our findings provide the foundation for further simulation studies involving mixed arginine/citrate overlayers with a goal of elucidating the AuNP assembly mechanisms. However, the system of pure arginine overlayers is already highly complex, and future simulations that incorporate the presence of citrate and/or AuNP edges and vertices will require further technical developments.

ASSOCIATED CONTENT

Supporting Information

Additional computational details, hydrogen-bonding data for the sparsely packed regime, average potential energies of overlayers as a function of annealing schedule, snapshots of the densely packed overlayers, total system potential energy as a function of simulation time, molecular structure of adsorbates, lateral water densities for the sparsely packed regime, schematic of the setup for the ordered overlayers, average heights of CA and CZ atoms in sparsely packed overlayers, number of waters inside the densely packed overlayers, lateral (2D) radial distribution functions in the densely packed regime, overlayer structural properties and hydrogen-bond autocorrelation functions. This material is available free of charge via the Internet at http://pubs.acs.org.

AUTHOR INFORMATION

Corresponding Author

*Phone: +61 (0)3 5227 3116. Fax: +61 (0)3 5227 1103. E-mail: tiffany.walsh@deakin.edu.au.

Notes

The authors declare no competing financial interest.

ACKNOWLEDGMENTS

The authors gratefully acknowledge the computing facilities of the Centre for Scientific Computing, University of Warwick. L.B.W. thanks the EPSRC for DTA studentship funding. This work was also supported by EPSRC Programme Grant (EP/I001514/1) Hard−Soft Matter Interfaces; From Understanding to Engineering. This work was partially supported by the Air Force Office of Scientific Research (Grant #FA9550-12-1-0226). T.R.W thanks **veski** for an Innovation Fellowship.

REFERENCES

(1) Daniel, M. C.; Astruc, D. Gold Nanoparticles: Assembly, Supramolecular Chemistry and Quantum-size-related Properties, and Applications Towards Biology, Catalysis, and Nanotechnology. *Chem. Rev.* **2004**, *104*, 293−346.

(2) Prats-Alfonso, E.; Albericio, F. Functionalization of Gold Surfaces: Recent Developements and Applications. *J. Mater. Sci.* **2011**, *46*, 7643−7648.

(3) Coppage, R.; Slocik, J. M.; Briggs, B. D.; Frenkel, A. I.; Heinz, H.; Naik, R. R.; Knecht, M. R. Crystallographic Recognition Controls Peptide Binding for Bio-based Nanomaterials. *J. Am. Chem. Soc.* **2011**, *133*, 12346−12349.

(4) Naik, R. R.; Stringer, S. J.; Agarwal, G. A.; Jones, S. E.; Stone, M. O. Biomimetic Synthesis and Patterning of Silver Nanoparticles. *Nat. Mater.* **2002**, *1*, 169−172.

(5) Slocik, J. M.; Stone, M. O.; Naik, R. R. Synthesis of Gold Nanoparticles using Multifunctional Peptides. *Small* **2005**, *1*, 1048−1052.

(6) Hnilova, M.; Oren, E. E.; Seker, U. O. S.; Wilson, B. R.; Collino, S.; Evans, J. S.; Tamerler, C.; Sarikaya, M. Effect of Molecular Conformations on Adsorption Behavior of Gold-binding Peptides. *Langmuir* **2008**, *24*, 12440−12445.

(7) Tamerler, C.; Kacar, T.; Sahin, D.; Fong, H.; Sarikaya, M. Genetically Engineered Polypeptides for Inorganics: A Utility in Biological Materials Science and Engineering. *Mater. Sci. Eng., C* **2007**, *27*, 558−564.

(8) Sethi, M.; Knecht, M. R. Experimental Studies on the Interactions Between Au Nanoparticles and Amino Acids: Bio-based Formation of Branched Linear Chains. *ACS Appl. Mater. Interfaces* **2009**, *1*, 1270−1278.

(9) Sethi, M.; Knecht, M. R. Understanding the Mechanism of Amino Acid Au Nanoparticle Chain Formation. *Langmuir* **2010**, *26*, 9860−9874.

(10) Durand-Gasselin, C.; Sanson, N.; Lequeux, N. Reversible Controlled Assembly of Thermosensitive Polymer-coated Solid Nanoparticles. *Langmuir* **2011**, *27*, 12329−12335.

(11) Wilson, K. E.; Fruchtl, H. A.; Grillo, F.; Baddeley, C. J. (S)-Lysine Adsorption Induces the Formation of Gold Nanofingers on Au(111). *Chem. Commun.* **2011**, *47*, 10365−10367.

(12) Mark, A. G.; Forster, M.; Raval, R. Recognition and Ordering at Surfaces: The Importance of Handedness and Footedness. *ChemPhysChem* **2011**, *12*, 1474−1480.

(13) Feyer, V.; Plekan, O.; Tsud, N.; Chab, V.; Matolin, V.; Prince, K. C. Adsorption of Histidine and Histidine-containing Peptides on Au(111). *Langmuir* **2010**, *26*, 8606−8613.

(14) Forster, M.; Dyer, M. S.; Persson, M.; Raval, R. 2D Random Organization of Racemic Amino Acid Monolayers Driven by Nanoscale Adsorption Footprints: Proline on Cu(110). *Angew. Chem., Int. Ed.* **2010**, *48*, 2344−2349.

(15) Robin, A.; Marnell, L.; Bjork, J.; Dyer, M. S.; Bermudez, P. S.; Haq, S.; Barrett, S. D.; Persson, M.; Minoia, A.; Lazzaroni, R.; Raval, R. Adsorption and Organisation of the Organic Radical on a Cu(110) Surface: A Combined STM, RAIRS and DFT Study. *J. Phys. Chem. C* **2009**, *113*, 13223−13230.
(16) Jones, G.; Jones, L. B.; Thibault-Starzyk, F.; Seddon, E. A.; Raval, R.; Jenkins, S. J.; Held, G. The Local Adsorption Geometry and Electronic Structure of Alanine on Cu(110). *Surf. Sci.* **2006**, *600*, 1924−1935.
(17) Zubavichus, Y.; Zharnikov, M.; Yang, Y.; Fuchs, O.; Hexks, C.; Umbach, E.; Tzvetkov, G.; Netzer, F. P.; Grunze, M. Surface Chemistry of Ultrathin Films of His on Au as Probed by High-resolution Synchrotron Photoemission. *J. Phys. Chem. B* **2005**, *109*, 884−891.
(18) Marti, E. M.; Quash, A.; Methivier, C.; Dubot, P.; Pradler, C. M. Interaction of S-Histidine, an amino acid, with Cu and Au Based on RAIRS. *Colloids Surf., A* **2004**, *249*, 85−89.
(19) Monti, S.; Li, C.; Carravetta, V. Reactive Dynamics Simulation of Monolayer and Multilayer Adsorption of Glycine on Cu(110). *J. Phys. Chem. C* **2013**, *117*, 5221−5228.
(20) Zhao, X.; Leng, Y.; Cummings, P. T. Self-Assembly of 1,4-Benzenedithiolate/Tetrahydrofuran on a Gold Surface: A Monte Carlo Simulation Study. *Langmuir* **2006**, *22*, 4116−4124.
(21) Sändig, N.; Zerbetto, F. Molecules on Gold. *Chem. Commun.* **2010**, *46*, 667−676.
(22) Ahn, Y.; Saha, J. K.; Schatz, G. C.; Jang, J. Molecular Dynamics Study of the Formation of a Self-Assembled Monolayer on Gold. *J. Phys. Chem. C* **2011**, *115*, 10668−10674.
(23) Kong, C. P.; Peters, E. A.; de With, G.; Zhang, H. X. Molecular Dynamics Simulation of a DOPA/ST Monolayer on the Au(111) Surface. *Phys. Chem. Chem. Phys.* **2013**, *15*, 15426−15433.
(24) Jha, K. C.; Liu, H.; Bockstaller, M. R.; Heinz, H. Facet Recognition and Molecular Ordering of Ionic Liquids on Metal Surfaces. *J. Phys. Chem. C* **2013**, *117*, 25969−25981.
(25) Almora-Barrios, N.; Novell-Leruth, G.; Whiting, P.; Liz-Marzan, L. M.; Lopez, N. Theoretical Description of the Role of Halides, Silver and Surfactants on the Structure of Gold Nanorods. *Nano Lett.* **2014**, *14*, 871−875.
(26) Rosa, M.; Corni, S.; di Felice, R. Enthalpy-Entropy Tuning in the Adsorption of Nucleobases at the Au(111) Surface. *J. Chem. Theory Comput.* **2014**, *10*, 1707−1716.
(27) Kruger, D.; Fuchs, H.; Rousseau, R.; Marx, D.; Parrinello, M. Pulling Monatomic Gold Wires with Single Molecules: An ab initio Simulation. *Phys. Rev. Lett.* **2002**, *89*, 186402.
(28) Hakkinen, H. The Gold-sulfur Interface at the Nanoscale. *Nat. Chem.* **2012**, *4*, 443−455.
(29) Jackson, A. M.; Myerson, J. W.; Stellacci, F. Spontaneous Assembly of Subnanometer Ordered Domains in the Ligand Shell of Monolayer Protected Nanoparticles. *Nat. Mater.* **2004**, *3*, 330−336.
(30) Singh, C.; Ghorai, P. K.; Horsch, M. A.; Jackson, A. M.; Larson, R. G.; Stellacci, F.; Glotzer, S. C. Entropy-mediated Patterning of Surfacant-coated Nanoparticles and Surfaces. *Phys. Rev. Lett.* **2007**, *99*, 226106.
(31) Causa, F.; della Modlie, R.; Laccino, E.; Mimmi, S.; Marasco, D.; Scognamiglio, P. L.; Battista, E.; Palmieri, C.; Cosenza, C.; Sanguigno, L.; et al. Evolutionary Screening and Adsorption Behavior of Engineered M13 Bacteriophage and Derived 12-peptide for the Selective Decoration of Gold Interfaces. *J. Colloid Interface Sci.* **2013**, *389*, 220−229.
(32) Brancolini, G.; Kokh, D. B.; Calzolari, L.; Wade, R. C.; Corni, S. Docking of Ubiquitin to Gold Nanoparticles. *ACS Nano* **2012**, *6*, 9863−9878.
(33) Iori, F.; Corni, S. Including Image Charge Effects in the Molecular Dynamics Simulations of Molecules on Metal Surfaces. *J. Comput. Chem.* **2008**, *29*, 1656−1666.
(34) Iori, F.; di Felice, R.; Molinari, E.; Corni, S. GoIP: An Atomistic Force-field to Describe the Interaction of Proteins with Au(111) Surfaces in Water. *J. Comput. Chem.* **2009**, *30*, 1465−1476.
(35) Hoefling, M.; Iori, F.; Corni, S.; Gottschalk, K.-E. Interaction of Amino Acids with the Au(111) Surface: Adsorption Free Energies from Molecular Dynamics Simulations. *Langmuir* **2010**, *26*, 8347−8351.
(36) Hoefling, M.; Iori, F.; Corni, S.; Gottschalk, K.-E. The Conformations of Amino Acids on the Gold(111) Surface. *ChemPhysChem* **2010**, *11*, 1763−1767.
(37) Hoefling, M.; Monti, S.; Corni, S.; Gottschalk, K. E. Interaction of Beta-sheet Folds with a Gold Surface. *PLoS One* **2011**, *6*, 20925.
(38) Heinz, H.; Vaia, R. A.; Farmer, B. L.; Naik, R. R. Accurate Simulation of Surfaces and Interfaces of fcc Metals using 12−6 and 9−6 LJ Potentials. *J. Phys. Chem. C* **2008**, *112*, 17281−17290.
(39) Heinz, H.; Farmer, B. L.; Pandey, R. B.; Slocik, J. M.; Patnaik, S. S.; Pachter, R.; Naik, R. R. Nature of Molecular Interactions of Peptides with Gold Palladium and Pd-Au Bimetallic Surfaces in Aqueous Solution. *J. Am. Chem. Soc.* **2009**, *131*, 9704−9714.
(40) Feng, J.; Pandey, R. B.; Berry, R. J.; Farmer, B. L.; Naik, R. R.; Heinz, H. Adsorption Mechanism of Single Amino Acid and Surfacant Molecules to Au(111) Surfaces in Aqueous Solution: Design Rules for Metal-binding Molecules. *Soft Matter* **2011**, *7*, 2113−2120.
(41) Wright, L. B.; Rodger, P. M.; Corni, S.; Walsh, T. R. GolP-CHARMM: First Principles Based Force-fields for the Interaction of Proteins with Au(111) and Au(100). *J. Chem. Theory Comput.* **2013**, *9*, 1616−1630.
(42) Wright, L. B.; Rodger, P. M.; Walsh, T. R.; Corni, S. First-Principles Based Force-Field for the Interaction of Proteins with Au(100)(5 × 1): An Extension of GolP-CHARMM. *J. Phys. Chem. C* **2013**, *117*, 24292−24306.
(43) Hughes, Z. E.; Wright, L. B.; Walsh, T. R. Biomolecular Adsorption at Aqueous Silver Interfaces: First-Principles Calculations, Polarizable Force-Field Simulations, and Comparisons with Gold. *Langmuir* **2013**, *29*, 13217−13229.
(44) Tang, Z.; Palafox-Hernandez, J. P.; Law, W.-C.; Hughes, Z. E.; Swihart, M. T.; Prasad, P. N.; Knecht, M. R.; Walsh, T. R. Biomolecular Recognition Principles for Bionanocombinatorics: An Integrated Approach to Elucidate Enthalpic and Entropic Factors. *ACS Nano* **2013**, *7*, 9632−9646.
(45) Li, H.-Q.; Chen, A.; Roscoe, S. G.; Lipkowski, J. Electrochemical and FTIR Studies of L-phenylalanine Adsorption at the Au(111) Electrode. *J. Electroanal. Chem.* **2001**, *500*, 299−310.
(46) Hess, B.; Kutzner, C.; van der Spoel, D.; Lindahl, E. Gromacs 4: Algorithms for Highly Efficient, Load Balanced, and Scable Molecular Simulation. *J. Chem. Theory Comput.* **2008**, *4*, 435−447.
(47) Jorgensen, W. L.; Maxwell, D. S.; Tirado-Rives, J. Development and Testing of the OPLS All-Atom Forcefield on Conformational Energetic and Properties of Organic Liquids. *J. Am. Chem. Soc.* **1996**, *118*, 11225−11236.
(48) Frens, G. Controlled Nucleation for the Regulation of the Particle Size in Monodisperse Gold Suspensions. *Nat. Phys. Sci.* **1973**, *241*, 20−22.
(49) Magnussen, O. M. Ordered Anion Adlayers on Metal Electrode Surfaces. *Chem. Rev.* **2002**, *102*, 679−725.
(50) Sethi, M.; Law, W.-C.; Fennell, W. A.; Prasad, P. N.; Knecht, M. R. Employing Materials Assembly to Elucidate Surface Interactions of Amino Acids with Au Nanoparticles. *Soft Matter* **2011**, *7*, 6532−6541.
(51) Hess, B. Determining the Shear Viscosity of Model Liquids from Molecular Dynamics Simulations. *J. Chem. Phys.* **2002**, *116*, 209−217.